Research Article

Tijana S. Kevkić*, Vojkan R. Nikolić, Vladica S. Stojanović, Dragana D. Milosavljević, and Slavica J. Jovanović

Modeling electrostatic potential in FDSOI MOSFETS: An approach based on homotopy perturbations

https://doi.org/10.1515/phys-2022-0012
received November 06, 2021; accepted January 26, 2022

Abstract: Modeling of the electrostatic potential for fully depleted (FD) silicon-on-insulator (SOI) metal-oxide-semiconductor field effect transistor (MOSFET) is presented in this article. The modeling is based on the analytical solution of two-dimensional Poisson's equation obtained by using the homotopy perturbation method (HPM). The HPM with suitable boundary conditions results in the so-called HPM solution in general and closed-form, independent of the surface potential. The HPM solution has been applied in modeling the output characteristics of the FDSOI MOSFET, which show good agreement compared with the numerical results.

Keywords: 2D Poisson equation, electrostatic potential, FDSOI MOSFETs, HPM, surface potential

*** Corresponding author: Tijana S. Kevkić,** University of Priština in Kosovska Mitrovica, Faculty of Sciences and Mathematics, Department of Physics, Lole Ribara 29, 38 220 Kosovska Mitrovica, Republic of Serbia, e-mail: tijana.kevkic@pr.ac.rs
Vojkan R. Nikolić: Department of Informatics, University of the Criminal Investigation and Police Studies, Cara Dušana 156, 11 000 Belgrade, Serbia, e-mail: vojkan.nikolic@kpu.edu.rs
Vojkan R. Nikolić: Department of Informatics, University of the Criminal Investigation and Police Studies, Cara Dušana 156, 11 000 Belgrade, Serbia, e-mail: vladica.stojanovic@kpu.edu.rs
Dragana D. Milosavljević: University of Priština in Kosovska Mitrovica, Faculty of Sciences and Mathematics, Department of Physics, Lole Ribara 29, 38 220 Kosovska Mitrovica, Republic of Serbia, e-mail: dragana82nis@yahoo.com, dragana.todorovic@pr.ac.rs
Slavica J. Jovanović: University of Priština in Kosovska Mitrovica, Faculty of Sciences and Mathematics, Department of Physics, Lole Ribara 29, 38 220 Kosovska Mitrovica, Republic of Serbia, e-mail: slavica.jovanovic@pr.ac.rs

Abbreviations

BCs	boundary conditions
BOX	buried oxide layer
DIBL	drain-induced barrier lowering
FD	fully depleted
HPM	homotopy perturbation method
ICs	integrated circuits
MOSFET	metal-oxide-semiconductor field effect transistor
SCEs	short channel effects
SOI	silicon-on-insulator
SS	subthreshold swing
V_{sub}	substrate bias (potential)
p	a homotopy parameter which takes value from zero to unit
$\mathcal{L}$	any integral or differential operator
$F(u)$	functional operator with known solutions v_0
L	the effective channel length
W	channel width
t_{ox}	gate oxide thickness
t_{Si}	silicon film thickness
t_{box}	buried oxide thickness
$\varphi(x, y)$	the potential distribution in silicon film
q	the electronic charge
N_A	the uniform film doping concentration independent of the gate length
ε_{Si}	the dielectric constant of silicon
$\varphi_s(x)$	the surface potential along the front interface of the Si film
V_G	gate voltage
ε_{ox}	the dielectric constant of the oxide
V_{fb}	the flat-band voltage between the channel and the front oxide layer
$V_{gs} = v = V_G - V_{fb}$	gate bias minus the flat-band voltage between the channel and the front oxide layer

$V_{fb,b}$	the flat-band voltage between the channel and the back oxide layer
$\varphi_b(x)$	potential along the bottom interfaces of Si film
$V_{gs,b} = V_{sub} - V_{fb,b}$	the substrate bias minus the flat-band voltage between the channel and the back oxide layer
$V_{bi} = u_T \ln\left(\frac{N_A N_D}{n_i^2}\right)$	the built-in voltage between source (drain) and the channel
u_T	the thermal voltage
N_D	the source/drain doping concentration
n_i	the intrinsic carrier concentration
$\lambda = l\sqrt{t_{Si}}$	the so-called natural length scale
V_{DS}	drain-to-source bias
$\Phi(x, y;p)$	homotopy function
μ_n	the carrier mobility
l_s	source–channel junction length
l_D	drain–channel junction length
I_d	drain current

1 Introduction

The most modern electronic products contain integrated circuits (ICs) based on silicon MOSFETs as they can perform various necessary functions efficiently and cheaply. The MOSFET is a unipolar transistor consisting of four terminals: source, gate, drain, and body. The body and the source terminals are sometimes connected together so that the MOSFET can be considered as a three-terminal device. The flow of minority charge carriers through a conducting channel between the source and the drain creates a current, which is controlled by a voltage applied to the gate. However, the gate control over the current flow in the channel is diminishing with shrinking the MOSFET's size imposed by continual IC technology advancement and the steady need to increase both performance and functionality while reducing power and cost. The MOSFETs downscaling has been carried out successfully until the 32 nm technological node when the short channel effects (SCEs) such as threshold voltage roll-off, drain-induced barrier lowering, and degradation of subthreshold swing (SS) relentlessly increased [1].

The elimination of these detrimental effects required increasing of the gate-channel capacitance and reducing of the charge sharing between the gate and drain in the channel [2]. For these reasons, the usage of the thinner gate oxide, as well as higher channel doping concentration, has been proposed [3]. However, it turned out that the reduction of the gate oxide thickness can lead to a large tunneling gate leakage current affecting the static power of the device. Additionally, the high-doping concentration can result in a decrease in the carrier mobility and an increase of the junction capacitance. To overcome these difficulties, the intensive research of innovative device structures that would show a superior short-channel immunity and ideal subthreshold characteristics has begun. As a suitable candidate that offers diminished SCEs, smaller SS, and mobility degradation, as well as a higher on-to-off current ratio compared to the conventional planar bulk, MOSFET emerged the fully depleted (FD) silicon-on-insulator (SOI) MOSFET [4].

As the traditional bulk devices, the FDSOI MOSFET is a four-terminal device: gate, source, drain, and body. The gate terminal is used to create an inversion charge whose carriers are supplied by source and drain wells, whereas a drop voltage between the source and drain terminals induces a field-effect current. Finally, in parallel to the gate terminal, the body terminal can be used to modulate and shift the charge in the channel and, therefore, affect the source-drain current. The primary innovation of the FDSOI MOSFET with respect to the planar bulk one is its layered SOI substrate, which could be described as a sandwich structure with an oxide layer, called the buried oxide (BOX), caught in the middle of two silicon layers. The upper silicon layer, also called SOI, is a thin film, which actually implements the transistor channel. Thanks to its thinness, there is no need to dope the channel, thus making the transistor FD. The presence of the BOX lowers the parasitic capacitance between the source and the drain and also efficiently confines the charge carriers flowing through the channel preventing any leakage currents into the substrate. The silicon substrate below the BOX is usually very lightly doped and can be depleted or inverted, depending on the applied voltage (V_{sub}).

From a modeling standpoint, one of the important questions is how to analytically calculate the characteristics of FDSOI MOSFET in an efficient and accurate way. Potential as the characteristic of a device that dominates the main mechanism of its operation is described by a two-dimensional (2D) Poisson equation. When the potential is obtained, the carrier density and the transport current can be accordingly derived. The various approaches of analytical solving the 2D Poisson equation for FDSOI MOSFET have been reported in the literature [5–9]. However, most of them are based on very strong assumptions and simplifications. For instance, an approximate analytical solution of the 2D Poisson equation by power series approach with neglecting higher-order terms of series is obtained in an earlier study [5]. However, previous

studies [6,7] give pseudo-2D solutions of the Poisson equation, whereas Guo and Wu [8] and Woo *et al.* [9] used a quasi-2D technique. Besides, most of the analytical and contemporary practical approaches [10–12] start from the same, Young's simple parabolic function [1] for the description of the potential distribution in the vertical direction.

In this study, for the first time, according to the available literature and our knowledge, the application of the homotopy perturbation method (HPM) for solving the 2D Poisson equation for the electrostatic potential problem of FDSOI MOSFET structures has been proposed. The HPM was developed by Ji-Huan He as a semianalytical technique for solving linear as well as nonlinear ordinary/partial differential equations and/or a system of coupled linear and nonlinear differential equations [13–34]. In recent years, the HPM has been widely used for solving Poisson equation for many problems in natural and engineering sciences [33–38]. For instance, exact and numerical solutions of the Poisson equation for electrostatic potential problems are given in an earlier study [35]. Moreover, the HPM has been applied to find the Poisson equation's exact solution with Dirichlet and Neumann boundary conditions (BCs) [36]. Furthermore, the HPM had been used to solve a nonlinear Singular Cauchy Problem of Euler–Poisson–Darboux equation [37], *etc*.

The innovative aspects of this research compared with previous related ones reflect in the HPM application for solving the 2D Poisson equation by considering certain BCs specific just for FDSOI MOSFET structure, as well as obtaining HPM solution in a very general form. Furthermore, the obtained HPM solution can be implemented in determination of the subthreshold drain current and compared to numerically obtained output characteristics of the considered device. Observed excellent agreements between them indicate the validity of introducing the HPM in FDSOI MOSFET modeling, as can be seen throwing the paper.

2 General HPM-procedure for solving 2D Poisson equation

The essential idea of HPM is the introduction of a homotopy parameter, p, which takes value from zero to unit. For $p = 0$, the equation or system of the equations usually reduces to a sufficiently simplified form whose solution can be readily obtained analytically. With gradual increases of parameter p to 1, the system goes through a sequence of "deformation," the solution of each of which is "close" to that at the previous stage of "deformation." Finally, when parameter p becomes equal to 1, the system of equations takes the required form, and the final stage of "deformation" gives the desired solution [39].

For a simple illustration of the basic concept of the HPM, we consider a general equation of the type,

$$\mathcal{L}(u) = 0, \tag{1}$$

where $\mathcal{L}$ is any integral or differential operator. A convex homotopy $H(u, p)$ is defined as follows:

$$H(u, p) = (1 - p)F(u) + \mathcal{L}(u), \tag{2}$$

where $F(u)$ is a functional operator with known solutions v_0.

The equation above exhibits specific behaviors at the limit values $p = 0$ and $p = 1$, as given in the following equation:

$$H(u, 0) = F(u),\ H(u, 1) = \mathcal{L}(u), \tag{3}$$

This shows that $H(u, p)$ continuously traces an implicitly defined curve from a starting point homotopy $H(v_0, 0)$ to a solution function $H(f, 1)$. The embedding parameter monotonically increases from 0 to 1 as the trivial problem $F(u) = 0$ continuously deforms the original problem $\mathcal{L}(u) = 0$. The embedding parameter $p \in (0, 1]$ can be considered as an expanding parameter [32]. The HPM uses the homotopy parameter, p, as the expanding parameter to obtain

$$u = \sum_{i=0}^{\infty} p^i u_i = u_0 + pu_1 + p^2u_2 + p^3u_3 + \ldots, \tag{4}$$

If $p \to 1$, then Eq. (4) corresponds to Eq. (2) and becomes the approximate solution of the form

$$f = \lim_{p \to 1} u = \sum_{i=0}^{\infty} u_i, \tag{5}$$

It is well known that series in Eq. (5) is convergent in most cases and also the rate of convergence is dependent on $\mathcal{L}(u)$. The comparisons of like powers of p give solutions of various orders.

In this section, the 2D Poisson equation for FDSOI MOSFET with appropriate BCs is defined, and then the general HPM-solution of the 2D Poisson equation is developed.

2.1 Formulation of the problem

The cross-sectional view of FD FDSOI MOSFET along the effective channel length L and width W is shown in Figure 1. The thickness of gate oxide is t_{ox}, the Si film, that is, channel is t_{Si}, and that of the BOX is t_{box}. The source–Si film and

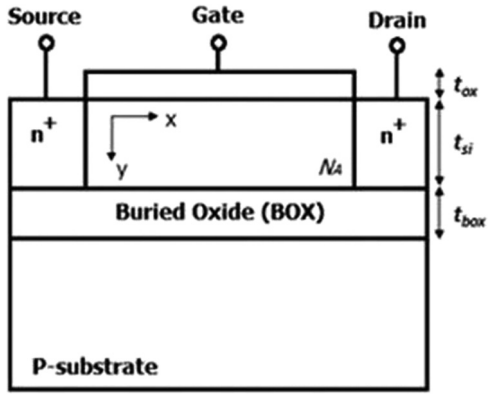

Figure 1: Cross-sectional view of a FDSOI MOSFET.

drain–Si film junctions are located at $x = 0$ and $x = L$, whereas the front and back interfaces the Si film–oxide are located at $y = 0$ and $y = t_{Si}$.

Assuming the impurity density in the channel region to be uniform and neglecting the effect of the fixed oxide charges on the electrostatics of the channel, the potential distribution in the Si film $\varphi(x, y)$ before the onset of strong inversion can be described by the 2D Poisson equation:

$$\frac{\partial^2\varphi(x,y)}{\partial x^2} + \frac{\partial^2\varphi(x,y)}{\partial y^2} = \frac{qN_A}{\varepsilon_{Si}}, \tag{6}$$

where $0 \le x \le L$ and $0 \le y \le t_{Si}$ are the direction parallel and perpendicular to the gate, respectively, and:

- q is the electronic charge,
- N_A is the uniform film doping concentration independent of the gate length, and
- ε_{Si} is the dielectric constant of silicon.

The BCs required for solving the 2D Poisson Eq. (6) can be given as follows:

(i) At $y = 0$ is valid:

$$\varphi(x, 0) = \varphi_s(x), \tag{7}$$

where $\varphi_s(x)$ is *the surface potential*, that is, the potential along the front interface of the Si film.

(ii) The electric field at $y = 0$ is determined by the gate voltage V_G and the gate oxide thickness, t_{ox}:

$$\left.\frac{\partial\varphi(x,y)}{\partial y}\right|_{y=0} = \frac{\varphi_s(x) - V_{gs}}{l^2} = g(x), \tag{8}$$

where we denoted that $l = \sqrt{t_{ox}\varepsilon_{Si}/\varepsilon_{ox}}$, $V_{gs} = V_G - V_{fb}$, and:

- ε_{ox} is the dielectric constant of the oxide and
- V_{fb} is the flat-band voltage between the channel and the front oxide layer.

(iii) The electric field at $y = t_{Si}$ is approximately:

$$\left.\frac{\partial\varphi(x,y)}{\partial y}\right|_{y=t_{Si}} = \frac{V_{gs,b} - \varphi_b(x)}{l_b^2} = o(t_{Si}), \tag{9}$$

when $t_{Si} \approx 0$. Here, $\varphi_b(x) = \varphi(x, y)$ is the back–channel potential, $l_b = \sqrt{t_{box}\varepsilon_{Si}/\varepsilon_{ox}}$, $V_{gs,b} = V_{sub} - V_{fb,b}$, and:

- V_{sub} is the substrate bias and
- $V_{fb,b}$ is the flat-band voltage between the channel and the back oxide layer.

Additionally, in the x direction are valid the following BCs:

(iv) The both of (electrostatic and surface) potentials at the source end, when $x = 0$, satisfy equality:

$$\varphi(0, 0) = \varphi_s(0) = V_{bi} - V_{gs} + \frac{qN_A}{\varepsilon_{Si}}\lambda^2, \tag{10}$$

where:

- $V_{bi} = u_T \ln\left(\frac{N_A N_D}{n_i^2}\right)$ is the built-in potential across the body–source junctions,
- u_T is the thermal voltage,
- N_D is the source/drain doping concentration,
- n_i is the intrinsic carrier concentration, and
- $\lambda = l\sqrt{t_{Si}}$ is the so-called natural length scale.

(v) The both of potentials at the drain end, when $x = L$, satisfy equality:

$$\varphi(L, 0) = \varphi_s(L) = V_{DS} + V_{bi} - V_{gs} + \frac{qN_A}{\varepsilon_{Si}}, \tag{11}$$

where V_{DS} is the applied drain–source bias.

2.2 HPM-solution of the 2D Poisson equation

Here, we start from the description of the general HPM procedure for solving the 2D Poisson Eq. (6), by using the first two BCs (i) and (ii), respectively. In that purpose, we introduce *the homotopy function*:

$$\Phi(x, y; p) = \sum_{j=0}^{\infty} p^j \varphi_j(x, y), \tag{12}$$

for which we assume that satisfies the homotopy equation:

$$p\frac{\partial^2\Phi(x,y;p)}{\partial x^2} + \frac{\partial^2\Phi(x,y;p)}{\partial y^2} = k, \tag{13}$$

where $k = qN_A/\varepsilon_{Si}$ and $p \in [0, 1]$ is *the embedding parameter*.

According to Eq. (12), when $p = 0$, the homotopy Eq. (13) becomes the so-called *initial equation*:

$$\frac{\partial^2\Phi(x,y;0)}{\partial y^2} = \frac{\partial^2\varphi_0(x,y)}{\partial y^2} = k. \tag{14}$$

After double integration on y, Eq. (14) gives *the initial solution*:

$$\varphi_0(x,y) = \frac{k}{2}y^2 + g(x)y + \varphi_s(x), \tag{15}$$

which obviously satisfies the BCs in Eqs. (7) and (8):

$$\begin{cases} \varphi_0(x,y)|_{y=0} = \varphi_s(x), \\ \dfrac{\partial\varphi_0(x,y)}{\partial y}\Big|_{y=0} = [ky + g(x)]|_{y=0} = g(x). \end{cases} \tag{16}$$

Let us notice that the obtained initial solution Eq. (15), which will serve for the determination of the final HPM-solution of the 2D Poisson Eq. (6), is the parabolic function such as Young's one [1].

However, when $p = 1$, the homotopy Eq. (13) becomes equivalent to the Poisson Eq. (6). In that case, according to Eq. (12), the HPM-solution of the 2D Poisson equation will be as follows:

$$\varphi(x,y) = \Phi(x,y;1) = \sum_{j=0}^{\infty}\varphi_j(x,y), \tag{17}$$

under the condition that the series in Eq. (17) converges.

Let us consider now the general case, when $0 < p < 1$. By substituting the homotopy function $\Phi(x,y;p)$ given by Eq. (12) into the homotopy Eq. (13), we obtain the following equation:

$$p\left[\sum_{j=0}^{\infty}p^j\frac{\partial^2\varphi_j(x,y)}{\partial x^2}\right] + \sum_{j=0}^{\infty}p^j\frac{\partial^2\varphi_j(x,y)}{\partial y^2} = k, \tag{18}$$

Alternatively, equivalently:

$$\frac{\partial^2\varphi_0(x,y)}{\partial y^2} + \sum_{j=1}^{\infty}p^j\left[\frac{\partial^2\varphi_j(x,y)}{\partial y^2} + \frac{\partial^2\varphi_{j-1}(x,y)}{\partial x^2}\right] = k. \tag{19}$$

From there, by equating the expression with identical powers p^j, $j = 0, 1, 2,\ldots$, the following equations get ones:

- When $j = 0$ apparently is obtained the initial Eq. (14):

$$\frac{\partial^2\varphi_0(x,y)}{\partial y^2} = k,$$

whose the (initial) solution is given by Eq. (15).

- In generally, arbitrary $j = 1, 2,\ldots$, yields the following recurrence equations:

$$\frac{\partial^2\varphi_j(x,y)}{\partial y^2} = -\frac{\partial^2\varphi_{j-1}(x,y)}{\partial x^2} = (-1)^j\left[g^{(2j)}(x)\frac{y^{2j-1}}{(2j-1)!} + \varphi_s^{(2j)}(x)\frac{y^{2j-2}}{(2j-2)!}\right], \tag{20}$$

After double integration on y, the solutions of Eq. (20) can be written in the following form:

$$\varphi_j(x,y) = (-1)^j\left[g^{(2j)}(x)\frac{y^{2j+1}}{(2j+1)!} + \varphi_s^{(2j)}(x)\frac{y^{2j}}{(2j)!}\right]. \tag{21}$$

In that way, the functions $\varphi_j(x,y)$ for each $j = 1, 2,\ldots$, satisfy the BCs:

$$\varphi_j(x,0) = \frac{\partial\varphi_j(x,y)}{\partial y}\Big|_{y=0} = 0. \tag{22}$$

Now, by replacing the previously obtained functions $\varphi_j(x,y)$, $j = 0, 1, 2,\ldots$, into the function given by Eq. (17), we obtain the *HPM solution* of the 2D Poisson Eq. (6) in the following general form:

$$\varphi(x,y) = \frac{ky^2}{2} + \sum_{j=0}^{\infty}(-1)^j\left[g^{(2j)}(x)\frac{y^{2j+1}}{(2j+1)!} + \varphi_s^{(2j)}(x)\frac{y^{2j}}{(2j)!}\right]. \tag{23}$$

Note that, according to Eqs. (16) and (23), the first two BCs given by Eqs. (7) and (8) are obviously fulfilled. Furthermore, in accordance with the second BC, given by Eq. (8), the function $g(x)$ has the derivatives of even order:

$$g^{(2j)}(x) = \frac{1}{l^2}\varphi_s^{(2j)}(x), \tag{24}$$

By replacing Eq. (24) into the HPM-solution given by Eq. (23), the general HPM-solution is as follows:

$$\varphi(x,y) = \frac{ky^2}{2} - \frac{vy}{l^2} + \left[\frac{1}{l^2}\sum_{j=0}^{\infty}(-1)^j\frac{y^{2j+1}}{(2j+1)!} + \sum_{j=0}^{\infty}(-1)^j\frac{y^{2j}}{(2j)!}\right]\varphi_s^{(2j)}(x). \tag{25}$$

where we labeled $v = V_{gs}$. As the obtained solution depends on the surface potential $\varphi_s(x)$, the above procedure will be hereinafter supplemented by certain specific forms of $\varphi_s(x)$, according to appropriate BCs.

3 The surface potential analysis

In this section, we will consider the third BC, given by Eq. (9). Let us notice that based on it directly follows:

$$\varphi_b(x) = \varphi(x, y)|_{y=t_{Si}} \approx V_{gs,b}, \tag{26}$$

that is, it is sufficient to observe an approximate equality:

$$\left.\frac{\partial\varphi(x, y)}{\partial y}\right|_{y=t_{Si}} \approx 0, \tag{27}$$

where $t_{Si} \approx 0$. By differentiation of Eq. (25) on $y = t_{Si}$, and by replacing in Eq. (27), we get the following:

$$kt_{Si} - \frac{v}{l^2} + \left[\frac{1}{l^2}\sum_{j=0}^{\infty}(-1)^j\frac{t_{Si}^{2j}}{(2j)!} + \sum_{j=1}^{\infty}(-1)^j\frac{t_{Si}^{2j-1}}{(2j-1)!}\right]\varphi_s^{(2j)}(x) \approx 0. \tag{28}$$

Thus, for every $n \in N$, the surface potential $\varphi_s(x)$ can be obtained as the approximate solution of the (second order) differential equation:

$$kt_{Si} - \frac{v}{l^2} + \left[\frac{1}{l^2}\sum_{j=0}^{n-1}(-1)^j\frac{t_{Si}^{2j}}{(2j)!} + \sum_{j=1}^{n}(-1)^j\frac{t_{Si}^{2j-1}}{(2j-1)!}\right]\varphi_s^{(2j)}(x) + O(t_{Si}^{2n}) \approx 0. \tag{29}$$

Let us consider, below, some concrete cases of approximate Eq. (29).

3.1 Second-order approximation

If we put $n = 1$, Eq. (29) becomes

$$kt_{Si} + \frac{\varphi_s(x) - v}{l^2} - t_{Si}\frac{d^2\varphi_s(x)}{dx^2} + O(t_{Si}^2) \approx 0. \tag{30}$$

Therefore, the surface potential $\varphi_s(x)$ can be obtained as a solution of the second-order differential equation:

$$\frac{d^2\varphi_s(x)}{dx^2} - \frac{\varphi_s(x)}{\lambda^2} = k - \frac{v}{\lambda^2}. \tag{31}$$

General solution of Eq. (31), already known in literature [40], is obtained in a simple way in the following form:

$$\varphi_s(x) = Ae^{x/\lambda} + Be^{-x/\lambda} + v - k\lambda^2. \tag{32}$$

Note that coefficients A, B can be easily determined from the additionally, x-direction BCs. Namely, by replacing the surface potential, given by Eq. (32), into the coupled Eqs. (10) and (11), we obtain the following equation:

$$\begin{cases} A + B = V_u \\ Ae^{L/\lambda} + Be^{-L/\lambda} = V_u + V_{DS} \end{cases}, \tag{33}$$

where $V_u = V_{bi} + k\lambda^2 - v$. By solving these equations with respect on A, B, the explicit expressions for these two coefficients are given as follows:

$$\begin{cases} A = \dfrac{V_u}{e^{L/\lambda} + 1} + \dfrac{V_{DS}}{e^{2L/\lambda} - 1}, \\ B = \dfrac{V_u e^{L/\lambda}}{e^{L/\lambda} + 1} + \dfrac{V_{DS} e^{L/\lambda}}{e^{2L/\lambda} - 1}. \end{cases} \tag{34}$$

However, the function $\varphi_s(x)$ has the even-order derivatives:

$$\varphi_s^{(2j)}(x) = \lambda^{-2j}(Ae^{x/\lambda} + Be^{-x/\lambda}), \tag{35}$$

where $j = 1, 2, \ldots$. Thus, substituting Eqs. (32) and (35) into the general HPM-solution given by Eq. (25), we obtain the following equation:

$$\varphi(x, y) = \frac{ky^2}{2} - \frac{vy}{l^2} + \left(\frac{y}{l^2} + 1\right)(v - k\lambda^2) + \frac{\lambda(Ae^{x/\lambda} + Be^{-x/\lambda})}{l^2}\sum_{j=0}^{\infty}(-1)^j\frac{(y/\lambda)^{2j+1}}{(2j+1)!} + (Ae^{x/\lambda} + Be^{-x/\lambda})\sum_{j=0}^{\infty}(-1)^j\frac{(y/\lambda)^{2j}}{(2j)!}. \tag{36}$$

Finally, it is obvious that Eq. (36), that is, *the HPM-solution of the 2D Poisson equation* can be written in the following analytic and closed form:

$$\varphi(x, y) = \frac{ky^2}{2} - kt_{Si}y + v - k\lambda^2 + (Ae^{x/\lambda} + Be^{-x/\lambda}) \times \left[\frac{t_{Si}}{\lambda}\sin(y/\lambda) + \cos(y/\lambda)\right]. \tag{37}$$

3.2 Fourth-order approximation

Similarly, as in the previous case, we put $n = 2$ in Eq. (29). The surface potential $\varphi_s(x)$ then represents the solution of the *fourth-order differential equation*:

$$\frac{d^4\varphi_s(x)}{dx^4} - m\frac{d^2\varphi_s(x)}{dx^2} + n\varphi_s(x) = \omega, \tag{38}$$

where

$$m = \frac{3(t_{Si}^2 + 2\lambda^2)}{\lambda^2 t_{Si}^2},\ n = \frac{6}{\lambda^2 t_{Si}^2},\ \omega = \frac{6(v - k\lambda^2)}{\lambda^2 t_{Si}^2}. \tag{39}$$

The general solution of Eq. (38) is as follows:

$$\varphi_s(x) = C_1 e^{\alpha x} + C_2 e^{-\alpha x} + C_3 e^{\beta x} + C_4 e^{-\beta x} + \gamma, \quad (40)$$

where $\pm\alpha$, $\pm\beta$ are the roots of the characteristic equation:

$$r^4 - mr^2 + n = 0, \quad (41)$$

and $\gamma = v - k\lambda^2$.

If we now put $C_1 = C_2 = A/2$ and $C_3 = C_4 = B/2$, the general solution of Eq. (38) can be written as follows:

$$\varphi_s(x) = A\cosh(\alpha x) + B\cosh(\beta x) + v - k\lambda^2. \quad (42)$$

The coefficients A, B, similarly as before, are obtained from the x-direction BCs, given by Eqs. (10) and (11). By replacing in these equations the function $\varphi_s(x)$, given by Eq. (42), we obtain the following equation:

$$\begin{cases} A + B = V_u, \\ A\cosh(\alpha L) + B\cosh(\beta L) = V_u + V_{DS}, \end{cases} \quad (43)$$

After solving these coupled equations with respect to A, B, it follows:

$$\begin{cases} A = \dfrac{V_{DS} + V_u[1 - \cosh(\beta L)]}{\cosh(\alpha L) - \cosh(\beta L)}, \\ B = \dfrac{V_{DS} + V_u[1 - \cosh(\alpha L)]}{\cosh(\beta L) - \cosh(\alpha L)}. \end{cases} \quad (44)$$

Finally, the function $\varphi_s(x)$ has the derivatives of the even order:

$$\varphi_s^{(2j)}(x) = \alpha^{2j} A\cosh(\alpha x) + \beta^{2j} B\cosh(\beta x), \quad (45)$$

where $j = 1, 2, \ldots$Thus, substitution of Eqs. (42) and (45) into Eq. (25) gives *the HPM-solution of the 2D Poisson equation*:

$$\varphi(x,y) = \frac{ky^2}{2} - kt_{Si}y + v - k\lambda^2 + A\cosh(\alpha x)\left[\frac{t_{Si}}{\alpha\lambda^2}\sin(\alpha y) + \cos(\alpha y)\right] + B\cosh(\beta x)\left[\frac{t_{Si}}{\beta\lambda^2}\sin(\beta y) + \cos(\beta y)\right]. \quad (46)$$

4 Results and discussions

As it is shown in previous section, the application of the HPM in solving 2D Poisson equation gives the electrostatic potential of thin Si film of FDSOI MOSFET in analytic and closed form, numbered as Eq. (37). To confirm the validity of the developed HPM procedure, we can now implement Eq. (37) into the expression for the drain current I_d of n channel FDSOI MOSFET, which operates in the subthreshold regime [41]:

Table 1: Applied voltages and relevant parameters

Items	Values
V_G	0.1000 V
V_{fb}	−0.4500 V
V_{DS}	1.000 V
V_{bi}	0.9500 V
v	0.5500 V
k	1.55×10^{13} V m^{-2}
l	6.7×10^{-5} m$^{1/2}$
λ	5.99×10^{-9} m

$$I_d = q\mu_n \frac{t_{Si}}{L} n_i u_T^2 (1 - e^{-V_{DS}/u_T}) \times \int_{-W/2}^{W/2} \int_{l_s - L/2}^{L/2 - l_D} e^{\frac{\varphi}{u_T}} dx\, dy. \quad (47)$$

where W is the channel width, μ_n is the carrier mobility, l_s and l_D are source–channel junction length and drain–channel junction length, respectively.

Further, we consider the n channel FDSOI MOSFET with following technologic characteristics: $L = 2 \times 10^{-8}$ m, $W = 10^{-8}$ m, $t_{Si} = 8 \times 10^{-9}$ m, $t_{ox} = 1.5 \times 10^{-9}$ m, $N_A = 10^{22}$ m^{-3}, and $N_D = 10^{26}$ m^{-3}. Also, the values of applied voltages and calculated values of parameters $v = V_{gs}$, k, l, and λ are listed in Table 1.

The procedure for calculating the subthreshold drain current I_d of considered device, with given values of applied voltages and relevant parameters, was implemented in a *Verilog A compact model code* and simulated in *QucsStudio 2.5.7 simulator*. Furthermore, the calculated I_d values are compared with the reference ones that contain the values of potential obtained by applying *Newton–Raphson algorithm* (Figure 2), similarly as in

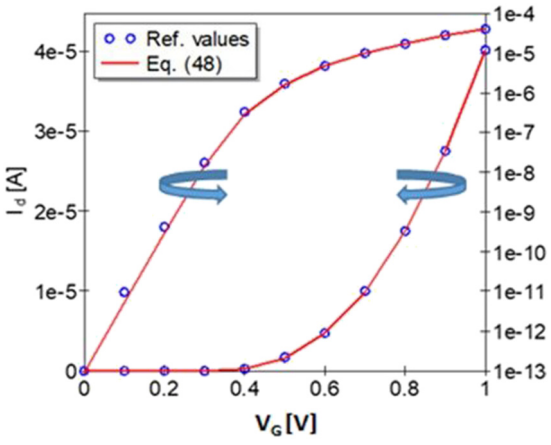

Figure 2: Subthreshold characteristic of considered FDSOI in linear and logarithmic scales.

Table 2: The results for drain current I_d in dependence of gate voltage V_G obtained by HPM and numerical procedure, both in linear and logarithmic scales

$V_G(V)$	Linear scale		Logarithmic scale	
	I_d (A) obtained by HPM	I_d (A) obtained by numerical procedure	I_d (A) obtained by HPM	I_d (A) obtained by numerical procedure
0.0	0.0	0.0	1.06865×10^{-13}	1.06865×10^{-13}
0.1	8.52834×10^{-6}	9.87751×10^{-6}	1.068651×10^{-13}	1.068651×10^{-13}
0.2	1.72498×10^{-5}	1.79605×10^{-5}	1.068652×10^{-13}	1.068652×10^{-13}
0.3	2.55737×10^{-5}	2.5923×10^{-5}	1.068653×10^{-13}	1.068653×10^{-13}
0.4	3.1922×10^{-5}	3.2199×10^{-5}	1.1748×10^{-13}	1.1748×10^{-13}
0.5	3.56081×10^{-5}	3.57527×10^{-5}	2.12039×10^{-13}	2.26698×10^{-13}
0.6	3.79451×10^{-5}	3.79451×10^{-5}	9.27995×10^{-13}	9.27995×10^{-13}
0.7	3.9499×10^{-5}	3.9499×10^{-5}	9.79338×10^{-12}	1.01262×10^{-11}
0.8	4.06314×10^{-5}	4.06314×10^{-5}	3.13164×10^{-10}	3.23808×10^{-10}
0.9	4.17396×10^{-5}	4.17396×10^{-5}	3.17261×10^{-8}	3.28044×10^{-8}
1.0	4.25106×10^{-5}	4.25106×10^{-5}	9.68487×10^{-6}	1.03544×10^{-5}

Table 3: Parameters values of the second-order and fourth-order surface potential approximations

Items	Parameters	
	Second order	Fourth order
A	4.93×10^{-2}	-7.67×10^{-2}
B	0.3512	0.4013
$\alpha[\mathrm{m}]^{-1}$	—	4.01×10^{8}
$\beta[\mathrm{m}]^{-1}$	—	1.27×10^{8}

earlier studies [42,43]. The plot in Figure 2 illustrates the drain current I_d of considered device *versus* gate voltage V_G, both in linear and logarithmic scales.

Good agreement between simulated results (lines) and numerical results (labeled by dots) in Figure 2 confirms the validity of the HPM approach and indicate that it can be used for deciding the important subthreshold characteristics of the device. For more accurate validation, the results obtained by HPM and numerical procedure of drain current I_d of the considered device *versus* gate voltage V_G, both in linear and logarithmic scales, are given in Table 2.

Let us emphasize once again that the obtained general HPM solution, that is, Eq. (25), depends on the surface potential $\varphi_s(x)$ for which, according to appropriate BCs, we determined two different forms, labeled by Eqs. (32) and (42), respectively. As, the explicit expression (32) is the solution of the second-order differential

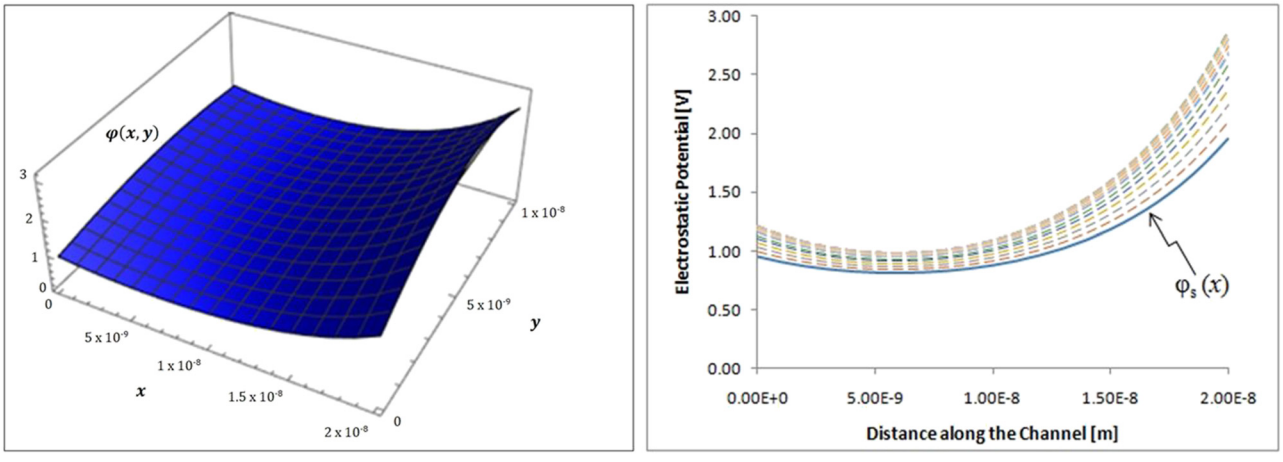

Figure 3: Results for the electrostatic potential $\varphi(x, y)$ with the second-order approximated the surface potential $\varphi_s(x)$: 3D plot of $\varphi(x, y)$ (left) and its trajectories in the y direction (right).

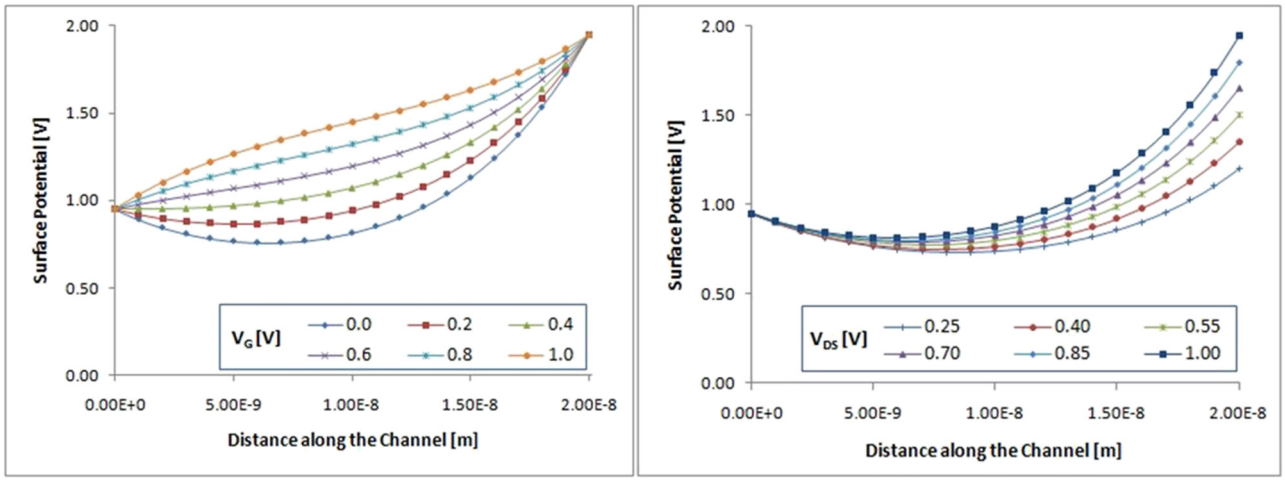

Figure 4: The second-order approximated surface potential $\varphi_s(x)$ *vs* distance along the channel for different values of the gate voltage V_G (left) and the drain-source voltage V_{DS} (right).

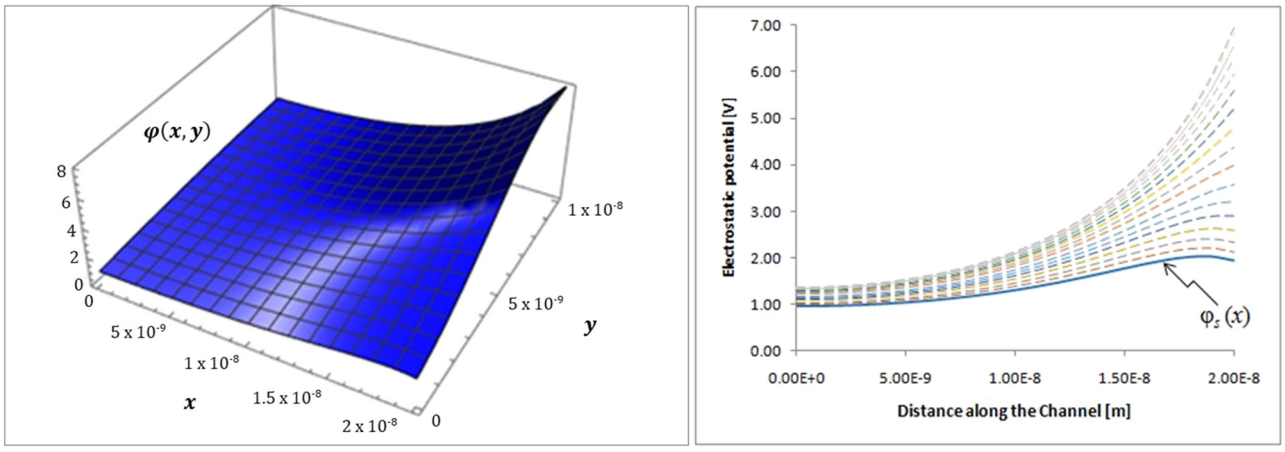

Figure 5: Results for the electrostatic potential $\varphi(x, y)$ with the fourth-order approximated surface potential $\varphi_s(x)$: 3D plot of $\varphi(x, y)$ (left) and its trajectories in the y direction (right).

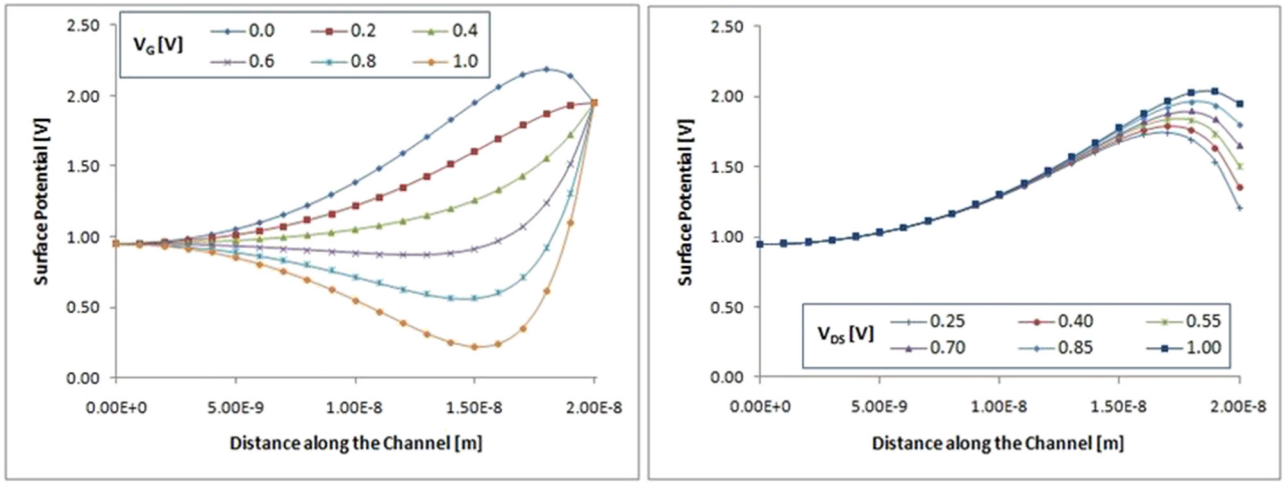

Figure 6: The fourth-order approximated surface potential $\varphi_s(x)$ *vs* distance along the channel for different values of the gate voltage V_G (left) and the drain-source voltage V_{DS} (right).

Eq. (31), it will be called *the second-order approximated surface potential*. In the same manner, Eq. (42) will be called *the fourth-order approximated surface potential* $\varphi_s(x)$. The values of coefficients, which appear in both of these approximated surface potential $\varphi_s(x)$, are given in Table 3.

After obtaining the functions $\varphi_s(x)$, the HPM solutions of the 2D Poisson equation can be easily determined through the Eqs. (37) and (46). As a result, the 3D plots of the HPM-solutions of the 2D Poisson equation with the second-order approximated $\varphi_s(x)$, given by Eq. (32), are shown in Figure 3. In the same figure (Figure 3), the electrostatic potential $\varphi(x, y)$ trajectories in y direction, with the solid line corresponding to the function $\varphi_s(x)$, are shown.

Further, the second-order approximated surface potential $\varphi_s(x)$ *vs* distance along the channel for the different values of the gate voltage V_G is presented in the left diagram in Figure 4. However, the right diagram in same figure (Figure 4) shows $\varphi_s(x)$ *vs* distance along the channel for the different values of the drain-source voltage V_{DS}.

Results for the electrostatic potential $\varphi(x, y)$ with the fourth-order approximated $\varphi_s(x)$, given by Eq. (42), are presented in Figure 5 (left), along with its y-direction trajectories (right).

In addition, the graphs of the fourth-order approximated surface potential $\varphi_s(x)$ *versus* distance along the channel for the different values of voltage V_G and V_{DS} are presented in Figure 6.

5 Conclusion

In this study, the analytical HPM solution of potential distribution for FDSOI MOSFET is achieved based on the solution of the 2D Poisson equation using proper BCs. Thereafter, the values of electrostatic potential, the surface potential and the drain current were calculated based on the derived HPM solution and have been compared with the numerical results. Good agreements with numerical data confirm the validity of the HPM approach and indicate that it can be used for the prediction of the important subthreshold characteristics of fully depleted SOI MOSFETs. As it is known, the determination of the subthreshold characteristic of FDSOI MOSFET is very important as it meets the present requirements of a transistor. That is why the accurate model for the electrostatic potential and consequently for subthreshold current represents the convenient tool from the FDSOI MOSFETs designer's point of view.

Acknowledgements: Authors thank the Ministry of Education, Science and Technological Development of the Republic of Serbia for support under Contract No. 451-03-9/2021-14, and the Faculty of Sciences and Mathematics in Kosovska Mitrovica (University of Priština in Kosovska Mitrovica, Department of Physics) for support under the project ИЈ-0201. Authors also thank their colleague Nenad Milojević, who provided the valuable suggestions on the article.

Funding information: Science and Technological Development of the Republic of Serbia for support under Contract No. 451-03-9/2021-14, and the Faculty of Sciences and Mathematics in Kosovska Mitrovica (University of Priština in Kosovska Mitrovica, Department of Physics) for support under the project ИЈ-0201.

Author contributions: All authors have accepted responsibility for the entire content of this manuscript and approved its submission.

Conflict of interest: The authors state no conflict of interest.

References

[1] Young KK. Short-channel effect in fully depleted SOI MOSFETs. IEEE T Electron Dev. 1989;36(2):399–402.
[2] Yan RH, Ourmazd A, Lee KF. Scaling the Si MOSFET: from bulk to SO1 to bulk. IEEE T Electron Dev. 1992;39(7):1704–10.
[3] Mohammadi H, Abdullah H, Dee CF. A review on modeling the channel potential in multi-gate MOSFETs. Sains Malays. 2014;43(6):861–6.
[4] Suzuki K, Tanaka T, Tosaka Y, Horie H, Arimoto Y. Scaling theory for double-gate SOI MOSFETs. IEEE T Electron Dev. 1993;40(12):2326–9.
[5] Su KW, Kuo JB. Analytical threshold voltage formula including narrow-channel effects for VLSI mesa-isolated fully depleted ultrathin silicon-on-insulator N-channel metal-oxide-silicon devices. Jpn J Appl Phys. 1995;34(8A):4010–9.
[6] Remmouchea R, Boutaoui N, Bouridah H. Compact modeling for submicron fully depleted SOI MOSFET's. Acta Phys Pol. 2012;121(1):190–2.
[7] Joachimet HO, Yamaguchi Y, Ishikawa K, Inoue Y, Nishimura T. Simulation and two dimensional analytical modeling of subthresholdslope in ultrathin-film SOI MOSFETs down to 0.1 μm gatelength. IEEE T Electron Dev. 1993;40(10):1812–7.
[8] Guo Y, Wu CY. A new 2-D analytic threshold voltage model forfully depleted short channel SOI MOSFETs. IEEE T Electron Dev. 1993;40(9):1653–61.

[9] Woo JCS, Terrill KW, Vasudev PK. Two dimensional analytic-modeling of very thin SOI MOSFETs. IEEE T Electron Dev. 1990;37(9):1999–2006.
[10] Reddy GV, Kumar MJ. A new dual-material Double-Gate (DMDG) nanoscale SOI MOSFET – Two-dimensional analytical modeling andsimulation. IEEE T Nanotechnol. 2005;4(2):260–8.
[11] Chakrabarti H, Maity R, Maity NP. Analysis of surface potential for dual-material-double-gate MOSFET based on modeling and simulation. Microsyst Technol. 2019;25:4675–84.
[12] Suddapalli SR, Nistala BR. A center-potential-based threshold voltage model for a graded-channel dual-material double-gate strained-Si MOSFET with interface charges. J Comput Electron. 2019;18(4):1173–81.
[13] He JH. Homotopy perturbation technique. Comput Method Appl M 1999;178(3–4):257–62.
[14] He JH. A coupling method of a homotopy technique and a perturbation technique for non-linear problems. Int J Nonlin Mech. 2000;3(1):37–43.
[15] He JH. Homotopy perturbation method: a new nonlinear analytical technique. Comput Math Appl. 2003;135(1):73–9.
[16] He JH. An elementary introduction to the homotopy perturbation method. Comput Math Appl. 2009;57(3):410–2.
[17] Zeb M, Haroon T, Siddiqui AM. Homotopy perturbation solution for flow of a third-grade fluid in helical screw rheometer. U Politeh Buch Ser A. 2014;76(4):179–90.
[18] Roy PK, Mallick A. Thermal analysis of straight rectangular fin using homotopy perturbation method. Alex Eng J. 2016;55(3):2269–77.
[19] Grysa K, Maciag A. Temperature dependent thermal conductivity determination and source identification or nonlinear heat conduction by means of the Trefftz and homotopy perturbation methods. Int J Heat Mass Tran. 2016;100:627–33.
[20] Kevkić T, Stojanović V, Randjelović D. Application of homotopy perturbation method in solving coupled Schrödinger and Poisson equation in accumulation layer. Rom J Phys. 2017;62(9–10):1–13. Article ID 122.
[21] Stojanović V, Kevkić T, Jelić G, Randjelović D. Determination of invariant measures: An approach based on homotopy perturbations. U Politeh Buch Ser A. 2018;80(2):119–28.
[22] Kevkić T, Stojanović V, Petković D. Solving Schrödinger equation for a particle in one-dimensional lattice: An homotopy perturbation approach. Rom Rep Phys. 2019;71(1):1–10. Article ID 101.
[23] Kevkić T, Stojanović V. Approximate solution of coupled Schrödinger and Poisson equation in inversion layer problem: An approach based on homotopy perturbations. Z Naturforsch A. 2019;74(6):457–67.
[24] Behera D, Chakraverty S. Numerical solution of fractionally damped beam by homotopy perturbation method. Open Phys. 2013;11(6):792–8.
[25] Marinca V, Ene RD. Optimal homotopy perturbation method for nonlinear differential equations governing MHD Jeffery-Hamel flow with heat transfer problem. Open Phys. 2017;15(1):42–57.
[26] Jafarimoghaddam A. On the homotopy analysis method (HAM) and homotopy perturbation method (HPM) for a nonlinearly stretching sheet flow of Eyring-Powell fluids. Eng Sci Technol. 2019;22(2):439–51.
[27] Javeed S, Baleanu D, Waheed A, Khan MS, Affan H. Analysis of homotopy perturbation method for solving fractional order differential equations. Math. 2019;7(1):1–40.
[28] Eladdad EE, Tarif EA. On the coupling of the homotopy perturbation method and new integral transform for solving systems of partial differential equations. Adv Math Phys 2019;2019(ID 5658309):1–7.
[29] Khan H, Mustafa S, Ali I, Kumam P, Baleanu D, Arif M. Approximate analytical fractional view of convection–diffusion equations. Open Phys. 2020;18(1):897–905.
[30] He JH, El-Dib YO. The enhanced homotopy perturbation method for axial vibration of strings. Facta UNIV-SER Mech. 2021;19(4):735–50.
[31] Qayyum M, Ismail F, Sohail M, Imran N, Askar S, Park C. Numerical exploration of thin film flow of MHD pseudo-plastic fluid in fractional space: utilization of fractional calculus approach. Open Phys. 2021;19(1):710–21.
[32] Khan A, Farooq M, Nawaz R, Ayaz M, Ahmad H, Abu-Zinadah H, et al. Analysis of couple stress fluid flow with variable viscosity using two homotopy-based methods. Open Phys. 2021;19(1):134–45.
[33] Makaew S, Neamprem K, Koonprasert S. Solving the Poisson process in conformable fractional calculus sense by homotopy perturbation method. Thai J Math. Special Issue: Annual Meeting in Mathematics 2019. 2019:387–399. Online ISSN 1686-0209.
[34] Chakraverty S, Mahato NR, Karunakar P, Rao TD. Advanced numerical and semi-analytical methods for differential equations. Chapter 12. Homotopy Perturbation Method. Hoboken, New Jersey: John Wiley&Sons Inc; 2019. p. 131–9. ISBN:9781119423461.
[35] Yıldırım S. Exact and numerical solutions of poisson equation for electrostatic potential problems. Math Probl Eng. 2008;2008(578723):1–11.
[36] Biazar J, Hosseini K, Gholamin P. Application of homotopy perturbation method to Poisson equation. J Appl Math.2006;3(9):33-7.
[37] Naderi R. Solving a nonlinear singular cauchy problem of Euler–Poisson–Darboux equation through homotopy perturbation method. Medbiotech J. 2019;3(2):29–34.
[38] Koshanova M, Turmetov B, Usmanov K. About solvability of some boundary value problems for poisson equation in the ball. Filomat. 2018;32(3):939–46.
[39] Mohyud-Din ST, Noor AM. Homotopy perturbation method for solving partial differential equations. Z Naturforsch A. 2009;64a:157–70.
[40] Kumar MJ, Orouji AA. Two-dimensional analytical threshold voltage model of nanoscale fully depleted SOI MOSFET with electrically induced S/D extensions. IEEE T Electron Dev. 2005;52(7):1568–75.
[41] Meel K, Gopal R, Bhatnagar D. Three-dimensional analytical subthreshold current model of fully depleted SOI MOSFET's. IJECET-Special Issue. 2013;(Special issue):74–9.
[42] Kevkić T, Stojanović V, Joksimović D. Application of generalized logistic functions in surface-potential-based MOSFET modeling. J Comput Electron. 2017;16(1):90–7.
[43] Kevkić T, Stojanović V, Joksimović D. Application of the generalized logistic functions in modeling inversion charge density of MOSFET. J Comput Electron. 2018;17(2):689–97.